Available online at www.sciencedirect.com

ScienceDirect

Geochimica et Cosmochimica Acta 278 (2020) 16–29

Geochimica et Cosmochimica Acta

www.elsevier.com/locate/gca

How mafic was the Archean upper continental crust? Insights from Cu and Ag in ancient glacial diamictites

Kang Chen [a,*], Roberta L. Rudnick [b,c], Zaicong Wang [a,d], Ming Tang [e], Richard M. Gaschnig [f], Zongqi Zou [a,d], Tao He [a,d], Zhaochu Hu [a,d], Yongsheng Liu [a,d]

[a] State Key Laboratory of Geological Processes and Mineral Resources, China University of Geosciences, Wuhan 430074, China
[b] Department of Earth Science and Earth Research Institute, University of California–Santa Barbara, Santa Barbara, CA 93106, United States
[c] Department of Geology, University of Maryland, College Park, MD 20742, United States
[d] School of Earth Sciences, China University of Geosciences, Wuhan 430074, China
[e] Department of Earth, Environmental and Planetary Sciences, Rice University, Houston, TX 77005, United States
[f] Department of Environmental, Earth and Atmospheric Sciences, University of Massachusetts Lowell, Lowell, MA 01854, United States

Received 7 March 2019; accepted in revised form 2 August 2019; available online 12 August 2019

Abstract

The concentrations of Cu and Ag, both insoluble chalcophile elements, can be used to place tight constraints on the proportion of basalts in the upper continental crust (UCC) through time via analyses of fine-grained terrigenous sedimentary rocks. Copper and Ag concentrations in magmas are largely controlled by sulfide dissolution during melting and sulfide fractionation during differentiation. We show that Cu is high in basalts but low in komatiites and felsic rocks, making Cu useful for constraining the proportion of basalts in the UCC. Furthermore, Cu/Ag ratios are high in basalts and komatiites but decrease with differentiation. The fine-grained matrix of ancient glacial diamictites shows dramatic declines in both Cu concentrations and Cu/Ag ratios at 3.0–2.4 Ga, after which diamictite Cu concentrations and Cu/Ag ratios remain roughly constant. Mass-balance calculations using average Cu concentrations of Archean komatiites, basalts and felsic rocks require that a high proportion basalt (65–75%) was present in the UCC at ~3.0 Ga, and this crust transitioned to a felsic-rock-dominated crust at ~2.4 Ga ago and has remained basically unchanged since then. This conclusion is supported by the consistency between the Cu/Ag ratios in the diamictites and the weighted average Cu/Ag ratios based on the lithological proportions obtained using Cu mass-balance calculations. Our observations document the emergence of felsic continental crust in the late Archean, which, in turn, indicates a fundamental change in Earth's dynamic regime at that time.

Keywords: Cu-Ag; Sulfide; Archean continental crust; Basalt proportion; Plate tectonics

1. INTRODUCTION

The chemical composition and lithological proportions of the emerged upper continental crust (UCC) shed light on the processes by which the continents formed (Rudnick, 1995), the timing of the onset of plate tectonics (Dhuime et al., 2015; Tang et al., 2016), and the chemical evolution of the atmosphere (Lee et al., 2016; Smit and Mezger, 2017) and the oceans (Konhauser et al., 2009). While it is widely accepted that the modern UCC is dominated by felsic rocks (Rudnick and Gao, 2003 and references therein), the composition of the Archean UCC is highly debated.

* Corresponding author.
E-mail address: kangchen@cug.edu.cn (K. Chen).

https://doi.org/10.1016/j.gca.2019.08.002
0016-7037/

Based on preserved exposures, the Archean UCC contained felsic rocks (both lavas and intrusions), basalts, and komatiites, but the original proportion of each rock type is unknown. Reconstructions based on preserved Archean crust carry large uncertainties due to preferential weathering of exposed mafic components (e.g., Condie, 1993; Horton et al., 1999; Zakharova et al., 2007). To alleviate the preservation bias in igneous records, fine-grained terrigenous sediments, which provide an average composition of the crust exposed to weathering and erosion, have been used to track average composition of insoluble elements in the UCC over time (e.g., Taylor and McLennan, 1985, and references therein). For example, Tang et al. (2016) used Ni/Co and Cr/Zn in terrigenous sediments to track the average MgO content of the UCC through time and found the average Archean UCC to be dominated by mafic and ultramafic lithologies (MgO > 11 wt.% before 3.0 Ga). Smit and Mezger (2017) reached a similar conclusion using Cr/U in terrigenous sediments. The longevity of this mafic continental crust is supported by the Hadean ^{142}Nd isotope signatures seen in Neoarchean granitic rocks (O'Neil and Carlson, 2017; Reimink et al., 2018).

The hypothesis of a mafic Meso- and Eoarchean continental crust was challenged by Greber et al. (2017), who used Ti isotopes in shales to infer that the UCC achieved a felsic bulk composition from the early Archean (>3.5 Ga ago). Greber et al. (2017) attributed the high Ni/Co and Cr/Zn ratios in terrigenous sediments to the incorporation of small amounts of Ni- and Cr-rich komatiites in a predominantly felsic crust. However, the robustness of Ti isotopes as a proxy for crustal differentiation was questioned by Deng et al. (2019), who showed that tholeiitic and calc-alkaline igneous differentiation suites follow different δ^{49}Ti–SiO_2 trends (δ^{49}Ti is the deviation in parts per thousand of the ^{49}Ti/^{47}Ti ratio relative to the Origins Laboratory Ti reference material), making the interpretation of δ^{49}Ti in shales in terms of SiO_2 non-unique. Recently, Greber and Dauphas (2019) argued that Al_2O_3/TiO_2 and Zr/TiO_2 ratios in terrigenous sediments can be used to estimate the SiO_2 content in the Archean UCC based on the relationship between these ratios and SiO_2 contents in igneous rocks, and argued that the Paleoarchean UCC (~3.25 Ga) was dominantly felsic.

A major difference between the felsic Archean UCC models (e.g., Greber et al., 2017) and the mafic Archean UCC models (e.g., Tang et al., 2016; Smit and Mezger, 2017) is the inferred proportion of basalt, which is low in the felsic models (10–20%) but high in the mafic models (40–80%). Here we use Cu concentration (denoted as [Cu]) and Cu/Ag ratio in glacial diamictites to constrain the proportion of basalt in the UCC over time.

In igneous rocks, Cu strongly partitions into sulfides (it is strongly chalcophile), but is nearly perfectly incompatible in silicate minerals (Ewart and Griffin, 1994; Adam and Green, 2006; Lee et al., 2012). Therefore, Cu concentrations in mantle-derived melts are primarily controlled by the exhaustion rate of sulfides during melting. Lee et al. (2012) showed that sulfide consumption begins during the initial melting of a peridotite, and thus, Cu behaves as a moderately incompatible element in incipient melting stages. As melting continues, [Cu] increases in the melt and decreases in the residue as the sulfide fraction is diminished. Aggregated melts reach maximum [Cu] after ~15–25% melting when sulfides in the residual peridotite are completely exhausted (Lee et al., 2012; Reekie et al., 2019). High degree partial melting (>25%) after sulfide exhaustion dilutes [Cu] in the melts. Therefore, basaltic melts that are generated by 5–20% partial melting (Wilson, 1989) tend to have high [Cu], whereas komatiites generated by 30–50% partial melting (Arndt, 2003) have low [Cu]. This sulfide effect in mantle-derived melts is borne out in the Archean mafic to ultramafic igneous database, which clearly shows increasing [Cu] with decreasing MgO at MgO > 8 wt.% (Fig. 1a). Some relatively low MgO basalts are sulfide-undersaturated differentiation products of high MgO basalts and komatiites, and partially contribute to the Cu-MgO trend at MgO > 8%. On the other hand, when basaltic magmas differentiate in the crust, sulfides may eventually saturate and fractionate, scavenging Cu and other chalcophile elements from the magmas (Fig. 1b) (Lee et al., 2012; Greaney et al., 2017; Jenner, 2017). Sulfide fractionation appears to be pervasive in Archean igneous differentiation suites, which show Cu depletion with decreasing MgO (MgO < 8 wt.%) and increasing SiO_2 (SiO_2 > 50 wt.%) (Fig. 1a, b). Sulfide control on magmatic [Cu] during both mantle melting and subsequent differentiation leads to conspicuously arcuate trends in Cu-MgO and Cu-SiO_2 plots. The average [Cu] in the UCC is thus particularly sensitive to the proportion of basalt, and by knowing the average [Cu] in the UCC over time, a mass balance can be used to calculate the relative proportions for komatiite, basalt, and felsic rocks.

In addition to [Cu], the Cu/Ag ratio in the UCC may also be useful to constrain the lithological proportions. It has been suggested that the Cu/Ag ratio is constant during mantle melting and MORB differentiation, indicating that only liquid sulfides with similar Cu and Ag partition coefficients are involved in these processes (Jenner et al., 2010, 2012; Wang and Becker, 2015; Wang et al., 2018a; Yang et al., 2018; Reekie et al., 2019). By contrast, Cu/Ag ratios decline significantly during late stage differentiation of arc-related magmas due to the fractionation of crystalline sulfides that have higher Cu partition coefficients than those of Ag (Jenner et al., 2010, 2012). Therefore, komatiites should have similar Cu/Ag as mantle peridotites and MORB, whereas felsic rocks that dominate the upper continental crust have low Cu/Ag that is comparable to modern felsic subduction-related magmas (e.g., Gao et al., 1998; Jenner et al., 2010, 2012). The Cu/Ag ratio is thus a useful proxy for tracking sulfide fractionation and lithological proportions in the protoliths of terrigenous sediments.

Estimates for the average Cu abundance in the present-day UCC show a relatively narrow range from 20 to 32 ppm (Rudnick and Gao, 2003 and references therein; Hu and Gao, 2008; Gaschnig et al., 2016). The Ag data for the present-day UCC are fewer, owing to the analytical challenges of analyzing Ag, but different estimates have yielded similar result (50–58 ppb) (Hamaguchi and Kuroda, 1959; Taylor and McLennan, 1985; Wedepohl, 1995; Gao et al., 1998). However, the abundances of the

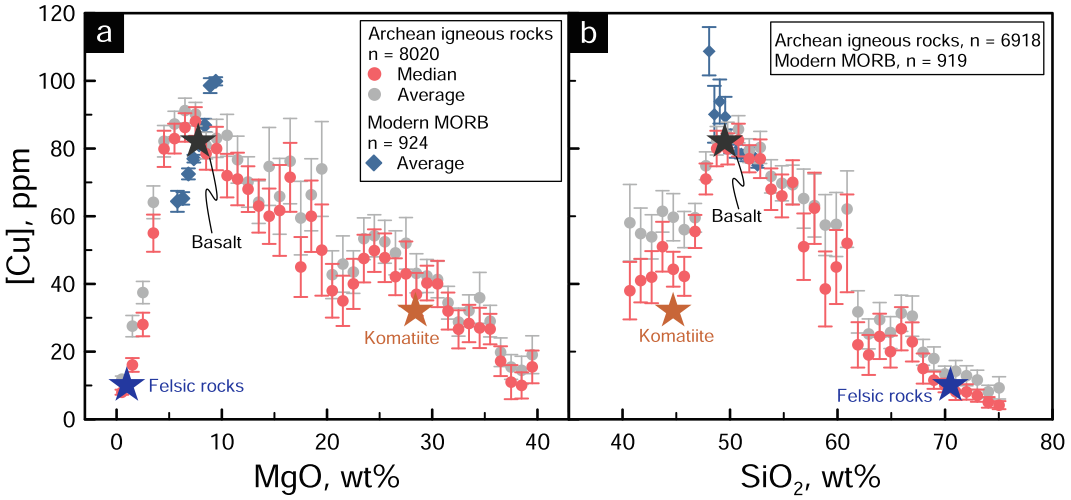

Fig. 1. Copper versus MgO (a) and SiO_2 (b) in Archean igneous rocks and modern MORB. Data for Archean igneous rocks are compiled from GEOROC (http://georoc.mpch-mainz.gwdg.de/georoc/Entry.html), and are binned by 1% MgO and SiO_2 contents, respectively. Data for MORB are from Jenner and O'Neill (2012) and Yang et al. (2018), and are binned by 0.5% MgO and SiO_2 contents, respectively. Within each bin, uncertainty at the 95% confidence interval around the median values is calculated using $(1.57 \times IQR)/\sqrt{N}$, where IQR = interquartile range (difference between third and first quartiles) and N = sample number within that bin. Error bars for average values are two standard deviations of the mean. Stars denote median values for komatiite, basalt and felsic rocks. We define komatiite as samples with MgO > 18 wt.%, basalt as samples with SiO_2 = 45–52 wt.% and MgO < 18 wt.%, and felsic rocks as samples with SiO_2 = 66–75 wt.%. We do not distinguish between different varieties of basalts (tholeiitic, calc-alkaline, alkalic, etc.). Note the higher [Cu] of basalt than komatiite and felsic rocks.

both elements in the ancient UCC have not yet been determined. In this work, we measured [Cu] and [Ag] in glacial diamictite composites to constrain the average [Cu] and Cu/Ag ratios in the UCC through time, which, in turn, allows quantification of the lithological proportions and UCC composition from the Mesoarchean to present.

2. SAMPLES

About 140 glacial diamictite samples were collected globally for four geological intervals (Fig. 2): Mesoarchean (~3.0 Ga), Paleoproterozoic (~2.2–2.5 Ga), Neoproterozoic (~0.58–0.75 Ga) and Paleozoic (~0.30 Ga). These samples are composed of a fine-grained matrix containing clasts of various shapes and sizes. Clasts were excluded to the best of our ability when generating the sample powder in order to access the fine-grained matrix (Gaschnig et al., 2016). The samples come from 24 stratigraphic units and, thus, 24 composite samples were made from the individual sample powders, with each composite representing one stratigraphic unit (Table 1). Detailed information about the stratigraphic units, the composite-making procedures, and whole rock geochemical data were reported by Gaschnig et al. (2014, 2016). Additional geochemical data are reported in the following papers: Chen et al. (2016) (Re-Os isotopes and platinum-group element concentrations); Li et al. (2016) (Li and Pb isotopes); Johnson and Goldblatt (2017) (N concentrations and N isotopes); Nan et al. (2018) (Ba isotopes); Mundl et al. (2018) (^{182}W isotopes); Wang et al. (2019) (Ni isotopes and total S content).

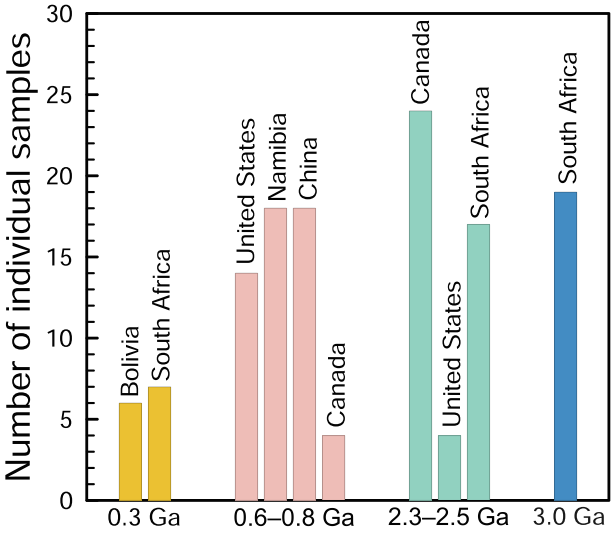

Fig. 2. Depositional age ranges and sample localities for individual diamictites.

The samples appear to be good proxies for tracking the chemical composition in the UCC through time (Gaschnig et al., 2014, 2016; Chen et al., 2016; Li et al., 2016). It should be noted that the Dwyka West composite, which was deposited in the Paleozoic, sampled mostly Archean crustal materials on the basis of detrital zircon ages (Gaschnig et al., 2014), and this Archean component is reflected in its whole rock composition.

3. ANALYTICAL TECHNIQUES

The Cu and Ag concentrations of the 24 composite samples were measured using isotope dilution ICP-MS, after HF-aqua regia digestion and ion exchange chromatogra-

Table 1
Basic information and data for selected major elements and Cu-Ag for diamictite composites.

Composite name	Sample location	Max. age, Ma	Min. age, Ma	SiO_2	Al_2O_3	Fe_2O_3T	MgO	CaO	Na_2O	K_2O	CIA*	Cu, ppm	2SE	Ag, ppb	2SE	$[Cu]_n$, ppm **	$[Ag]_n$, ppb **	Cu/Ag
Mozaan	S Africa	2980	2954	59.0	8.98	25.8	3.10	0.45	0.57	1.45	74	34.4	0.6	38.3	0.2	50.6	56.3	899
Afrikander	S Africa	2981	2935	65.2	8.70	8.65	9.59	6.23	0.58	0.61	77	44.4	0.6	19.6	0.1	67.3	29.8	2258
Promise	S Africa	2981	2935	72.6	11.4	9.81	2.73	0.83	0.66	1.52	75	49.9	0.7	22.4	0.2	57.8	26.0	2224
Coronation	S Africa	2981	2935	74.3	15.3	4.17	1.98	0.37	0.33	2.96	78	219	8	112	1	190	96.5	1965
Coronation (replicate)												220	10	112	1			
Duitschland	S Africa	2480	2310	60.1	16.0	13.1	2.99	3.13	0.09	3.27	82	10.7	0.1	63.1	0.4	10.3	60.7	170
Timeball Hill	S Africa	2256	2193	67.3	16.1	7.79	1.66	1.63	1.42	3.31	66	24.8	0.3	53.8	0.4	23.7	51.6	460
Makganyene	S Africa	2431	2222	61.2	8.96	19.9	4.27	3.63	0.06	1.09	89	31.8	0.5	59.1	0.4	54.6	102	538
Ramsay Lake	Canada (Ontario)	2450	2308	70.1	13.1	7.98	3.33	1.05	1.49	2.15	67	22.8	0.3	113	1	26.9	133	202
Bruce	Canada (Ontario)	2450	2308	69.4	15.1	4.65	3.27	0.36	3.81	2.77	61	2.56	0.06	7.00	0.03	2.61	7.13	366
Gowganda	Canada (Ontario)	2450	2308	67.3	15.0	6.50	2.66	0.95	4.74	2.04	57	18.7	0.3	26.0	0.2	19.1	26.6	720
Bottle Creek	USA (Wyoming)	2460	2090	72.3	13.6	4.26	2.54	0.53	4.22	1.94	58	41.8	0.6	8.29	0.04	47.5	9.41	5044
Gaskiers	Canada (Newfoundland)	581	580	68.5	15.3	5.32	1.70	1.18	3.67	3.36	57	16.3	0.2	55.6	0.4	16.4	56.0	293
Pocatello	USA (Idaho)	705	667	71.4	13.1	6.53	1.74	0.76	1.08	3.96	66	15.2	0.2	40.0	0.3	17.9	47.1	381
Konnarock	USA (Virginia)	760	570	69.2	14.3	5.37	1.53	1.23	2.76	4.55	56	11.4	0.1	23.3	0.1	12.3	25.1	489
Nantuo	China (Hubei)	655	635	68.8	15.1	5.95	2.54	1.92	1.33	3.49	65	29.2	0.4	21.6	0.1	29.9	22.1	1353
Gucheng	China (Hubei)	703	655	69.9	15.0	5.63	2.16	1.16	1.08	3.54	67	20.5	0.3	30.7	0.2	21.0	31.5	667
Blaubeker	Namibia	746	635	78.5	10.08	3.99	1.38	0.56	1.71	3.13	59	21.6	0.4	108	1	33.0	165	200
Kaigas	Namibia	771	741	66.1	15.6	6.28	2.47	2.28	2.71	3.45	57	30.8	0.5	15.3	0.1	30.3	15.0	2016
Chuos	Namibia	746	635	55.5	9.76	8.73	7.60	12.63	1.33	2.82	58	20.5	2.2	26.7	0.1	32.3	42.1	767
Numees	Namibia	741	555	72.8	13.0	3.82	1.56	1.99	2.03	4.02	54	15.8	0.2	11.8	0.1	18.7	13.9	1343
Ghaub	Namibia	637	633	42.3	9.54	4.43	3.97	35.44	0.79	2.87	64	14.1	0.2	16.0	0.1	22.7	25.9	878
Ghaub (replicate)												14.6	0.3	19.4	0.1			
Bolivia	Bolivia	326	299	76.3	12.7	4.01	1.64	0.42	1.14	2.90	70	6.8	0.2	54.1	0.4	8.22	65.4	126
Dwyka East	S Africa	312	288	69.0	14.2	5.56	2.35	1.61	3.24	3.04	56	19.5	0.3	50.5	0.4	21.1	54.6	387
Dwyka West	S Africa	312	288	51.2	10.47	11.68	9.58	12.44	1.08	2.06	65	44.6	0.6	120	1	65.6	177	371

Copper and Ag data are from this study. Other information and data are from Gaschnig et al. (2016).
*CIA = chemical index of alteration ($Al_2O_3/(Al_2O_3 + CaO + K_2O + Na_2O)$) where CaO has corrected to remove contributions from apatite and carbonate.
**Cu and Ag concentrations are normalized to the average Al_2O_3 contents of the Archean (13.2%) and post-Archean (15.4%) upper continental crust. $[Cu]_n = [Cu]_{sam} \times Al_2O_{3UCC}/Al_2O_{3sam}$. $[Ag]_n = [Ag]_{sam} \times Al_2O_{3UCC}/Al_2O_{3sam}$.

phy, at the State Key Laboratory of Geological Processes and Mineral Resources, China University of Geosciences, Wuhan. For each composite sample, about 0.2 g sample powder was weighed into a Teflon Parr bomb along with 1 mL concentrated HNO_3, 3 mL concentrated HF and appropriate amounts of ^{65}Cu-^{109}Ag spikes. After fitted tightly into an outer stainless-steel pressure jacket, the bomb was heated at 190 °C for 72 hours in an oven. The sample solution, after cooling to room temperature, was transferred into a 15 mL PFA vial and evaporated on a hot plate at 80–90 °C. Two mL concentrated HNO_3 were added to the salt and evaporated to dryness again. Then a mixture of 1 mL concentrated HNO_3 and 3 mL concentrated HCl was added into the vial. The vial, which was wrapped with Teflon tape prior to use to improve sealing, was capped tightly and heated on a hot plate at 160 °C for 24 hours to decompose possible remaining organic materials. The aqua regia was dried down and converted to chloride by adding 3 mL 6 mol L^{-1} HCl. The HCl was evaporated to dryness and the HCl fluxing was repeated. Finally, the salt was dissolved in 1.5 mL 4.5 mol L^{-1} HCl, and the sample solution was transferred into a centrifuge tubes and centrifuged.

Detailed procedures for ion exchange chromatography closely followed Wang et al. (2015). Briefly, two columns were used: Column A, 2 mL AG1-X8 anion exchange resin, and Column B, 1 mL AG1-X8 anion exchange resin. Two fractions, containing Cu and Ag, respectively, were obtained after Column A separation, eluted by 8 mL 0.4 mol L^{-1} HCl and 8 mL 9 mol L^{-1} HCl, respectively. The Ag fraction was dried down and diluted in 2% HNO_3 for ICP-MS measurements. The Cu fraction was dried down and dissolved in 0.8 mL HCl-ascorbic mixture (0.4 ml 9 M HCl + 0.4 ml 0.15 g/ml ascorbic acid). After loading on Column B, Cu was eluted by 4.5 mL 0.4 mol L^{-1} HCl. Finally, the Cu solution was dried down and diluted in 2% HNO_3 for ICP-MS measurements.

Isotopic ratios were measured by a single collector, sector field, inductively coupled plasma mass spectrometer (*Thermo Scientific Element XR*) with an electron multiplier detector. The ICP-MS was fitted with a Twinnabar cyclonic spray chamber (*Glass Expansion*) and a 0.1 mL/min Micro-Mist EzyFit nebulizer (*Glass Expansion*). To resolve molecular and oxide interferences, the $^{65}Cu/^{63}Cu$ ratios were measured at a medium resolution mode ($m/\Delta m = 4000$), in which the Ti oxide interferences on ^{63}Cu and ^{65}Cu can be easily resolved. Furthermore, Ti signal intensities are negligible for all our measurements ($^{47}Ti/^{63}Cu < 0.003$) owing to the effective purification. Accordingly, no interference corrections were made for Cu measurements. The $^{109}Ag/^{107}Ag$ ratios were determined in a low resolution mode. The ^{91}Zr and ^{93}Nb were monitored because of their potential oxide interferences on Ag. The oxide yields for ^{91}Zr and ^{93}Nb are 2% and 0.5%, respectively, and the $^{91}Zr/^{107}Ag$ and $^{93}Nb/^{109}Ag$ ratios of all our measurements are <0.02 and <1, respectively. Therefore, these oxide interferences are negligible and no correction was made.

Five total procedural blanks were analyzed during the whole analyses campaign. The averages were 10 ± 12 ng and 27 ± 31 pg (2SD) for Cu and Ag, respectively. The blank contributions are <1% for Cu (excluding the Bruce composite, where it is 2%), and <1% for Ag (again excluding the Bruce for which the blank contribution was 1.9%, the Bottle Creek at 1.6% and Numees at 1.1%). Blank corrections were made for all samples. Reference materials UB-N (serpentinite), BHVO-2 (basalt), and SBC-1 (shale) were analyzed as unknowns along with the diamictites. As shown in Table 2, our Cu results are in good agreement with published values. Reported Ag concentrations for the three reference materials vary widely (Table 2). Our Ag results agree well with those reported by Wang et al. (2015), which used similar analytical method to this study. Two replicates (the Coronation and the Ghaub composites) were analyzed and the two samples replicated well (Table 1). The [Cu] for diamictite composites obtained by Gaschnig et al. (2016) using conventional method of external standard agree well with our [Cu] results using isotope dilution method (Fig. A1), with deviations less than 15% (excluding the Duitschland composite for which the deviation is 30%, the Bruce at 18% and Chuos at 19%).

4. RESULTS

The Cu and Ag concentration data for the diamictite composites are listed in Table 1. Some diamictites are enriched in one or more particular types of minerals such

Table 2
Copper and Ag results for reference materials.

Reference materials	This study							Published values	
								GeoRem	Wang et al. (2015)
UB-N (serpentinite)	Digestion-1	Digestion-2	Digestion-3			Average	2SD		
Cu, ppm	24.9 ± 0.4	26.1 ± 0.3	24.5 ± 0.1			25	2	25 ± 5	23 ± 2
Ag, ppb	45.3 ± 0.3	43.7 ± 0.3	44.5 ± 0.1			45	2	45–79	45 ± 2
BHVO-2 (basalt)	Digestion-1	Digestion-2	Digestion-3	Digestion-4	Digestion-5				
Cu, ppm	133 ± 2	128 ± 3	131 ± 3	124 ± 2	123 ± 2	128	9	129 ± 1	129 ± 1
Ag, ppb	43.7 ± 0.3	44.4 ± 0.3	44.1 ± 0.3	43.8 ± 0.3	44.4 ± 0.3	44.1	0.6	44.5–1540	44.5 ± 0.8
SBC-1 (shale)	Digestion-1	Digestion-2							
Cu, ppm	31.2 ± 0.4	29.1 ± 0.7				30	3	31 ± 6	
Ag, ppb	71.1 ± 0.5	67.9 ± 0.5				70	5	180–900	

Uncertainties for the individual digestion analyses from this study are two standard deviation of the mean propagated from the measured isotopic ratios and two standard deviations for the average and published values. Note the anomalously large ranges of reported Ag values for BHVO-2 and SBC-1.

as carbonate, Fe-oxide, or quartz, resulting in anomalously high contents of CaO (and/or MgO), Fe_2O_{3T} (total iron as Fe_2O_3) and SiO_2, respectively. All of these minerals are depleted in Cu and Ag, so their enrichments dilute the bulk [Cu] and [Ag] (as well as Al_2O_3) relative to the original igneous crust composition. To account for this dilution effect, we followed Taylor and McLennan (1985) and Gaschnig et al. (2016), and normalized the measured [Cu] and [Ag] in the diamictites to the average content of Al_2O_3 of the UCC, using the following formulae: $[Cu]_n = [Cu]_{sam}*Al_2O_{3UCC}/Al_2O_{3sam}$, and $[Ag]_n = [Ag]_{sam}*Al_2O_{3UCC}/Al_2O_{3sam}$, where 'sam' = concentration in sample; 'UCC' = concentration in average UCC.

The rationale for this normalization scheme is as follows. First, the average Al_2O_3 contents for the Archean and post-Archean UCC has been well constrained. This is because the variation of Al_2O_3 contents from mafic to felsic igneous rocks is relatively small, with medians ranging from 13.9 to 14.6% in the Archean and from 14.5 to 15.7% in the post-Archean; Archean komatiites have an average Al_2O_3 content of ~5.0 wt.% (Table 3). Hence, the average Al_2O_3 contents for the UCC through time are independent of the basalt/felsic rock ratio, but will be affected by the presence of komatiite. It has been suggested that there was ~10% komatiite in the Archean UCC and post-Archean komatiite is rare (Arndt et al., 2008). Based on these lithological proportions and their average Al_2O_3 contents (Table 3), the average Al_2O_3 contents of the Archean UCC and post-Archean UCC are calculated to be 13.2 wt.% and 15.1 wt.%, respectively. The latter is similar to the estimates of the modern UCC (15.4 wt.%, Rudnick and Gao, 2003), whereas the former is slightly lower than that estimated by Taylor and McLennan (1985, 15.3 wt.%), because their Archean UCC was created by mixing felsic and mafic Archean igneous rocks without considering a komatiite contribution. Note that if we were to adopt the Taylor and McLennan value for average Al_2O_3 in the Archean UCC, the resulting [Cu] and [Ag] concentrations in Archean rocks would be slightly higher than those shown in Table 1 and plotted in the figures. Secondly, Al is insoluble and should not be significantly affected by chemical weathering processes (Taylor and McLennan, 1985). Therefore, fine-grained sediments that sampled large areas of the continental surface, if homogenized sufficiently, should

Table 3
Compilation of Cu, Al_2O_3, SiO_2 and MgO in komatiites, basalts and felsic rocks in the Archean and post-Archean.

		Archean			Post-Archean	
	Average/Median	Komatiite	Basalt	Felsic rocks	Basalt	Felsic rocks
Cu	**Median, ppm**	**32**	**82**	**10**	**68.0**	**7.3**
	Q1	15	52	5	46	4.0
	Q3	54	115	24	100	15.0
	95% confidence interval	1	2	1	0.7	0.2
	Average, ppm	39	87	16	74.8	10.9
	2SE	1	2	1	0.6	0.2
	N	1794	1903	695	13,366	8718
Al_2O_3	**Median, wt.%**	**4.97**	**13.90**	**14.62**	**15.73**	**14.50**
	Q1	3.50	12.60	13.78	14.70	13.65
	Q3	6.70	14.80	15.39	16.71	15.20
	95% confidence interval	0.09	0.06	0.07	0.02	0.02
	Average, wt.%	5.11	13.61	14.48	15.71	14.40
	2SE	0.07	0.05	0.06	0.01	0.01
	N	2955	3654	1388	29,538	23,196
SiO_2	**Median, wt.%**	**44.7**	**49.50**	**70.5**	**48.86**	**70.71**
	Q1	42.1	48.47	68.9	47.74	68.84
	Q3	46.5	50.42	72.3	50.03	72.50
	95% confidence interval	0.1	0.05	0.1	0.02	0.04
	Average, wt.%	44.3	49.41	70.6	48.87	70.65
	2SE	0.1	0.04	0.1	0.02	0.03
	N	2923	3654	1396	29,740	23,619
MgO	**Median, wt.%**	**28.4**	**7.76**	**0.97**	**6.78**	**0.550**
	Q1	24.7	6.50	0.65	5.60	0.340
	Q3	32.7	9.64	1.47	7.90	0.870
	95% confidence interval	0.2	0.08	0.03	0.02	0.006
	Average, wt.%	28.9	8.23	1.10	6.77	0.626
	2SE	0.2	0.07	0.03	0.02	0.005
	N	3355	3654	1385	29,740	22,291

Median values (**bold**) are used in the mass-balance calculations. We limit the definitions of komatiite to samples with MgO of >18 wt.%, basalt to samples with SiO_2 of 45–52 wt.% and MgO of <18 wt.%, and felsic rocks to samples with SiO_2 of 66–75 wt.%. Archean igneous data are compiled from GEOROC (http://georoc.mpch-mainz.gwdg.de/georoc/Entry.html) and post-Archean igneous data are from Keller et al. (2015). Uncertainty at the 95% confidence interval around the median values is calculated using $(1.57 \times IQR)/\sqrt{N}$, where IQR = interquartile range (difference between third and first quartiles, denoted as Q3 and Q1, respectively) and N = sample number. Uncertainties for average values are two standard deviations of the mean.

have similar Al_2O_3 content to the corresponding average UCC Al_2O_3 content. Third, those sediments with lower Al_2O_3 content than the average UCC mainly reflect a dilution effect resulting from the enrichment of the Al-depleted phases mentioned above. Thus, when these low Al_2O_3 sediments are used to estimate the average igneous UCC composition, this dilution effect needs to be compensated for by normalizing their Al_2O_3 contents to average UCC Al_2O_3 contents, otherwise underestimates may be produced. Therefore, as described above and in the caption to Table 1, we normalized Mesoarchean diamictites to Al_2O_3 of 13.2 wt.%, and post-Archean diamictites to 15.4 wt.%, the average Al_2O_3 content of modern UCC.

The [Cu] and [Ag] in the samples from the Mozaan, Afrikander, Makganyene, Chuos and Ghaub composites are diluted either by carbonates or Fe-oxides. The dilution factors for these samples are about 1.5. For all the other samples, the dilution factors are between 0.8–1.2. In the following paragraphs and figures of this study, unless otherwise indicated, all [Cu] and [Ag] are based on the UCC-Al_2O_3-normalized concentrations. These normalized concentrations are designated as $[Cu]_n$ and $[Ag]_n$.

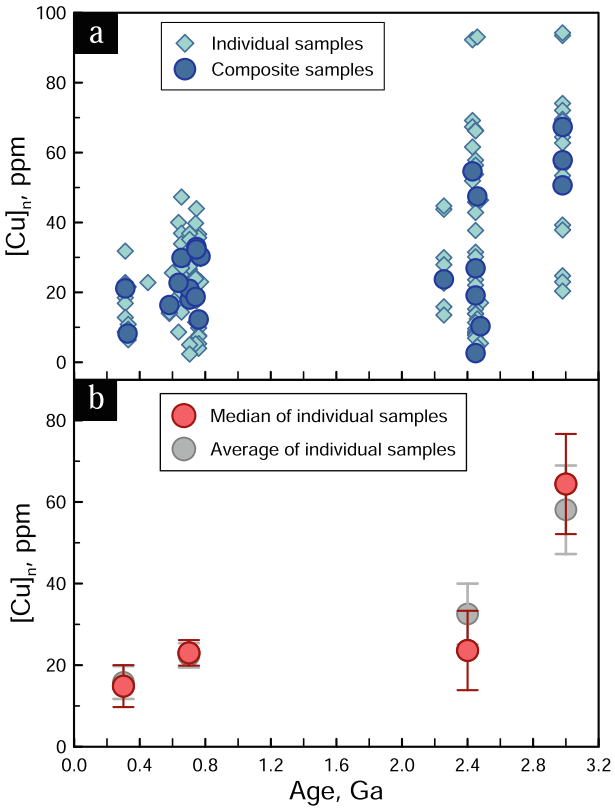

Fig. 3. (a) UCC-Al_2O_3-normalized [Cu] ($[Cu]_n$) of individual and composite diamictites versus maximum depositional ages. Data for individual samples are from Gaschnig et al. (2016). Copper data in the individual samples from the Paleozoic Dwyka West Group were not plotted because their provenance materials have an Archean age (Gaschnig et al., 2014, 2016). (b) Median and average $[Cu]_n$ of individual diamictites versus maximum depositional ages. The Coronation composite has an anomalously high $[Cu]_n$ of 190 ppm, probably caused by one individual sample in this Formation with an extremely high $[Cu]_n$ of 771 ppm. Both the composite and the individual Coronation samples were not plotted. This individual sample was also not incorporated in calculation of the median and average $[Cu]_n$ for the Mesoarchean (Table 4); adding it would produce even higher $[Cu]_n$ for the Mesoarchean UCC. Median and average values are listed in Table 4. Error bars for median and average values are calculated following the methods introduced in Fig. 1.

The $[Cu]_n$ of composite samples, together with the $[Cu]_n$ of individual samples reported by Gaschnig et al. (2016), are plotted versus maximum depositional ages in Fig. 3. The $[Ag]_n$ for composite samples versus depositional ages are presented in Fig. A2. The Neoproterozoic and Paleozoic diamictites have restricted values of $[Cu]_n$ and $[Ag]_n$, ranging from ~8 to ~33 ppm, and from ~13 to ~65 ppb, respectively (excluding the Blaubeker, which has a very high $[Ag]_n$ of 165 ppb, but a 'normal' $[Cu]_n$ of 33 ppm). Although the $[Cu]_n$ values for Paleoproterozoic samples are slightly more scattered than the younger samples (Neoproterozoic and Paleozoic), they have similar average and median values, within uncertainty, as the younger ones. By contrast, the Mesoarchean samples, though heterogeneous, have systematically higher median (64 ppm) and average (58 ppm) $[Cu]_n$ than the younger samples (Table 4, Fig. 3). The Paleoproterozoic and Mesoarchean samples show a large range of $[Ag]_n$, from 7.13 ppb to 133 ppb. About one third of the Paleoproterozoic and Mesoarchean samples have higher $[Ag]_n$ than the younger samples (Fig. A2). Like the secular variation of $[Cu]_n$, average and median Cu/Ag ratios also decrease from the Mesoarchean (~2,100) to the Paleoproterozoic (~400), and no obvious change is observed between the Paleoproterozoic and younger samples (Table 4, Fig. 4). The significant variations in Cu and Ag concentrations in Mesoarchean and Paleoproterozoic diamictites likely reflects greater lithological heterogeneity in the Archean UCC, and poorer homogenization of these lithologies during the processes of sedimentation. This observation is similar to the variability of REE and other lithophile trace elements observed in Archean shales (Taylor and McLennan, 1985).

5. DISCUSSION

5.1. Evaluating diamictites as representative samples of the average UCC

Previous studies have demonstrated that the glacial diamictites, though reflecting local geology in their chemical compositions, also show consistent temporal trends for key elements and elemental ratios that transcend these regional influences (Gaschnig et al., 2014, 2016; Chen et al., 2016). We now evaluate whether the [Cu] and [Ag] in these glacial diamictites were affected by chemical weathering processes. Chemical weathering can be quantified using CIA values (CIA = molar $Al_2O_3/(Al_2O_3 + K_2O + Na_2O + CaO^*)$ (Nesbitt and Young, 1982), where CaO* is CaO associated with the silicate fraction of the bulk sample (McLennan, 1993)), which range between 54 and 89 in the diamictite composites (Table 1). These values are slightly to significantly higher than those of average igneous rocks, which have CIA < 55. This observation,

Table 4
Diamictite Cu concentrations (ppm) and Cu/Ag ratios in each epoch.

Epoch	**Median Cu of individual diamictites**	Average Cu of individual diamictites	Median Cu of composite diamictites	Average Cu of composite diamictites	**Median Cu/Ag of composite diamictites**	Average Cu/Ag of composite diamictites
Mesoarchean	**64**	58	58	59	**2100**	1800
Uncertainty	**12**	11	15	10	**600**	600
no.	**17**	17	3	3	**4**	4
Paleoproterozoic	**24**	33	24	26	**400**	400
Uncertainty	**10**	7	22	14	**200**	200
no.	**43**	43	7	7	**6**	6
Neoproterozoic	**23**	22	22	23	**700**	800
Uncertainty	**3**	3	6	5	**500**	400
no.	**53**	53	10	10	**10**	10
Paleozoic	**15**	16	15	15	**200**	200
Uncertainty	**5**	4	14	13	**200**	200
no.	**14**	14	2	2	**2**	2

Median values for Cu concentrations from the individual diamictites and Cu/Ag ratios from compostie diamctites (**bold**) are used in the mass-balance calculations. Anomalously high Cu concentration of the Mesoarchean Coronation composite and high Cu/Ag ratio of the Paleoproterozoic Bottle Creek composite in the Paleoproterozoic are not incorporated. Copper data in the individual samples from the Paleozoic Dwyka West Group and Cu and Ag data for this composite sample were not incorporated because most of their source materials have an Archean age.

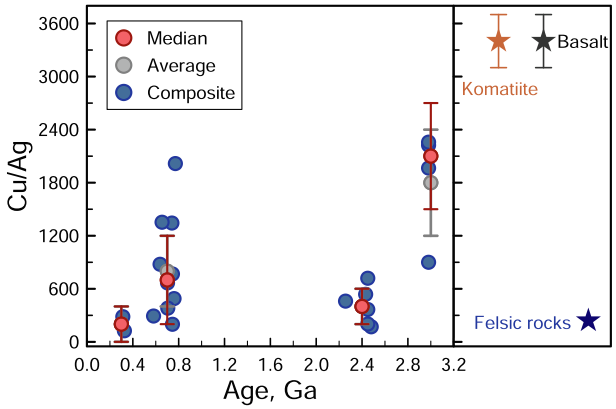

Fig. 4. Cu/Ag ratios for diamictite composites versus maximum depositional ages. The Cu/Ag ratios for komatiite, basalt and felsic rocks are also plotted for comparison. Median and average Cu/Ag ratios for composite samples, listed in Table 4, are calculated within each time period. Error bars for median and average values are calculated following the methods introduced in the caption of Fig. 1. The Paleoproterozoic Bottle Creek composite has an anomalously high Cu/Ag of 5044, even higher than mantle values, thus is not incorporated in the calculation of the median and average values. The Cu/Ag ratios for komatiite and basalt are assumed to have similar values to the mantle (see text for explanation). The Cu/Ag ratio for felsic rocks is the median value from Gao et al. (1998) (Table A1).

coupled with the systematic depletion in Sr, and their relatively low δ^7Li (Gaschnig et al., 2014, 2016; Li et al., 2016), demonstrate that the diamictites contain a weathered component. This component was interpreted to be principally inherited from weathered regolith that the glaciers removed as they traversed the continents (Gaschnig et al., 2016; Li et al., 2016).

Copper is a relatively insoluble element and should not be influenced by chemical weathering. For example, it has a relatively short seawater residence time (5000 years, Boyle et al., 1977). Moreover, studies of weathering profiles developed on Phanerozoic granites, granodiorites, and basalts show little perturbation of Cu during incipient to advanced chemical weathering (Fig. A3) (Middelburg et al., 1988; Nesbitt and Wilson, 1992; Nesbitt and Markovics, 1997; Wang et al., 2018b). Additionally, the concentrations of soluble elements in the younger diamictites (e.g., Na and Sr, Fig. 5a, b) typically show negative correlations with CIA. Such a correlation is not seen between $[Cu]_n$ and CIA (Fig. 5c). Collectively, we suggest that $[Cu]_n$ in diamictites is a good proxy for average $[Cu]_n$ in the UCC.

The solubility of Ag during incipient to advanced chemical weathering of unmineralized crustal rocks (e.g., granitoid, basalt) has yet to be investigated, due largely to the analytical challenges in analyzing Ag. However, the lack of correlation between $[Ag]_n$ and CIA values in the younger diamictites (Fig. 5d), coupled with its short seawater residence time (350 years, Broecker and Peng, 1982) suggest limited Ag mobility during chemical weathering.

5.2. Secular variations and mass balance

5.2.1. Mass balance based on Cu

As shown in Fig. 3, $[Cu]_n$ in both individual diamictites and composite samples decreases from the Mesoarchean to the Paleoproterozoic, after which there is no obvious change. The student's *t*-test shows that, statistically, the difference between Mesoarchean and Paleoproterozoic samples is significant, whereas there is only a slight difference between Paleoproterozoic and younger samples (Table A2). We calculated the median and average $[Cu]_n$ for the Mesoarchean, Paleoproterozoic, Neoproterozoic

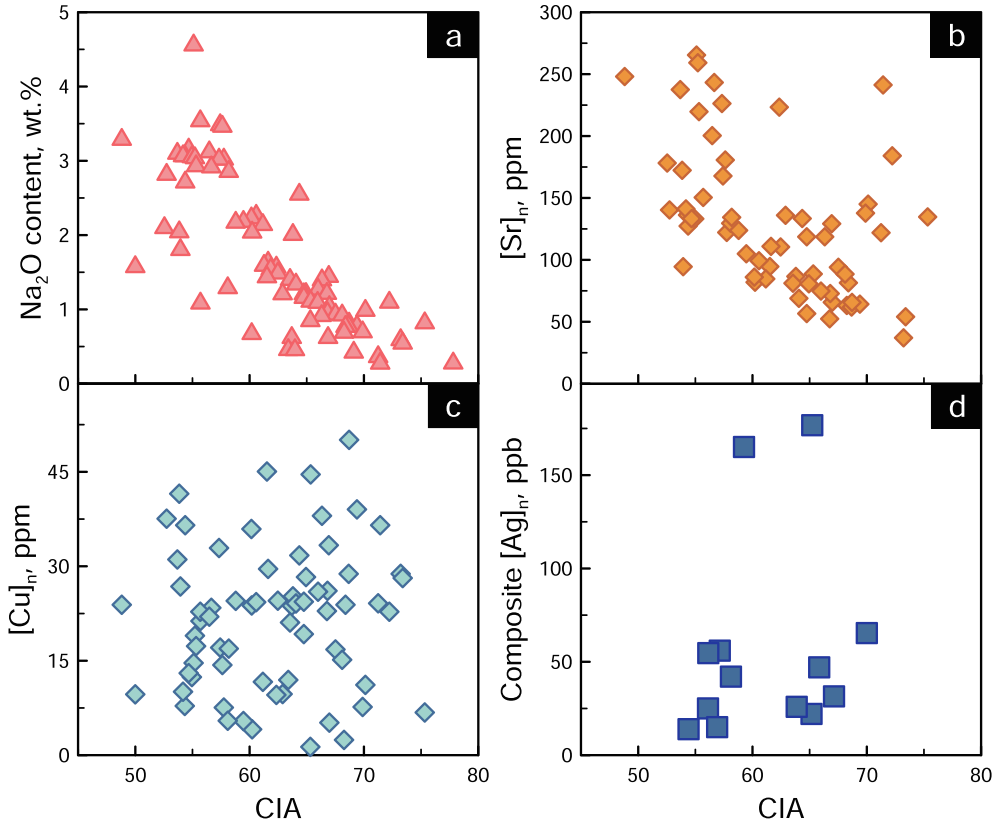

Fig. 5. CIA values versus Na_2O (a), Sr (b), Cu (c), and Ag (d) for Neoproterozoic and Paleozoic diamictites. Na_2O, Sr, Cu data are for individual diamictites (Gaschnig et al., 2014, 2016) and Ag data are for composite diamictites. Mesoarchean and Paleoproterozoic diamictites are not plotted as the compositions of the crust sampled by these older diamictites may be different from that of the modern UCC, and thus influence the concentrations of the ordinate elements. All three trace elements are normalized to the Al_2O_3 content of the modern UCC (15.4 wt.%), following the methods described in the text. Three anomalously high Sr samples (400–2200 ppm), which contain significant carbonate, are not plotted.

and Paleozoic individual samples, which are internally consistent and within uncertainty of the median and average values of composite samples (Table 4).

Mesoarchean diamictites have a median $[Cu]_n$ of 64 ± 12 ppm, which is much higher than both Archean komatiites (~32 ppm) and felsic rocks (~10 ppm) and only lower than Archean basalts (~82 ppm) (Table 3). Such high [Cu] requires a significant amount of basalt to be present in the Mesoarchean UCC. Diamictite $[Cu]_n$ drops to 24 ± 10 ppm in the Paleoproterozoic, which suggests that the UCC became predominantly felsic by the end of the Archean. We now evaluate the lithological proportions in the UCC and its bulk composition through time based on Cu mass balance:

$$F_k C_k^{Cu} + F_b C_b^{Cu} + F_f C_f^{Cu} = C_{UCC} \quad (1)$$

$$F_k + F_b + F_f = 1 \quad (2)$$

where F_k, F_b and F_f are the mass proportions of komatiite, basalt and felsic rocks in the UCC; C_{UCC} is the Cu abundance in the UCC for a given time, which is estimated from $[Cu]_n$ of the diamictites (Table 4), and C_k^{Cu}, C_b^{Cu} and C_f^{Cu} are the average [Cu] concentrations for komatiites, basalts and felsic rocks, respectively. Average [Cu] of these three lithologies in the Archean and the latter two lithologies in the post-Archean are listed in Table 3.

Because the Mesoarchean diamictite $[Cu]_n$ is higher than the average [Cu] of Archean komatiite and felsic rocks, the mass proportion of komatiite (F_k) in the Mesoarchean UCC must be lower than ~36%, otherwise the mass proportion of felsic rocks will be negative (Fig. 6). Similarly, the mass proportion of felsic rocks (F_f) cannot exceed ~25%. The maximum bounds on komatiite and felsic rock mass proportions lead to a mass proportion of basalt (F_b) in the range of 65%–75% in the Mesoarchean UCC (Fig. 6). Similar calculations can be done for the post-Archean UCC, which, in the absence of komatiites ($F_k = 0$) (Condie, 1994; Arndt et al., 2008), requires felsic rocks to be the dominant lithology (~70%) from the Paleoproterozoic to the present.

5.2.2. Further constraints from Cu/Ag ratios

The secular change of Cu/Ag ratios in the UCC may be used to test the UCC evolution model based on Cu mass balance. Copper and Ag have been suggested to behave similarly during mantle melting and MORB differentiation, as evidenced by the similar Cu/Ag ratios in the primitive mantle, fertile lherzolites, pyroxenites, plateau basalts,

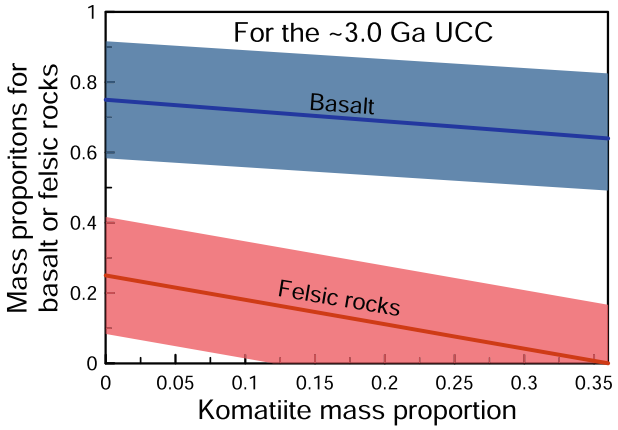

Fig. 6. Calculated mass proportions of basalt and felsic rocks as functions of komatiite mass proportion in the Mesoarchean UCC. Shaded areas are the uncertainty fields propagated from uncertainty of the Mesoarchean UCC Cu abundance (64 ± 12 ppm, Table 4).

mid-ocean ridge basalts (MORBs), Hawaiian basalts, and primitive arc-related magmas, all of which have Cu/Ag falling within a narrow range of 2500–4000 (Fig. 7) (Jenner et al., 2010, 2012; Jenner and O'Neill, 2012; Wang and Becker, 2013, 2015; Greaney et al., 2017; Wang et al., 2018a; Yang et al., 2018; Reekie et al., 2019). Although limited Ag data exist for komatiites and basalts (excluding MORBs), we speculate that primitive (high MgO content)

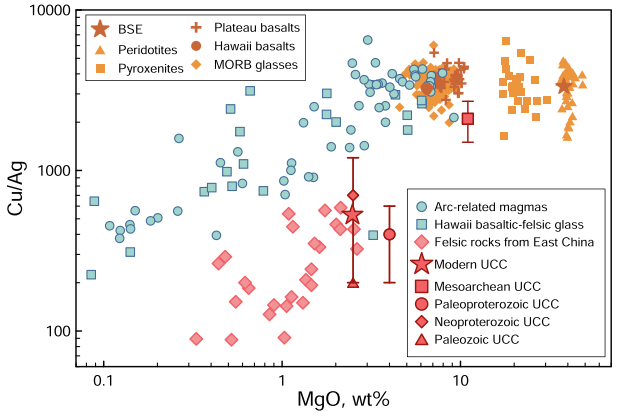

Fig. 7. Cu/Ag ratios versus MgO content for different lithologies and reservoirs. Data sources are as follows: bulk silicate earth (BSE) from Wang and Becker (2015); peridotites from Wang and Becker (2013, 2015); pyroxenites from Wang et al. (2018a); Ontong Java plateau basalts from Reekie et al. (2019), MORB glasses from Jenner and O'Neill (2012) and Yang et al. (2018); Hawaii basalts from Jenner et al. (2012); arc-related magmas from Jenner et al. (2010, 2012); Hawaii mafic-felsic glasses from Greaney et al. (2017); felsic rocks from East China from Gao et al. (1998); modern UCC from sources cited in Rudnick and Gao (2003). The Cu/Ag ratios for the Mesoarchean, Paleoproterozoic and modern UCC are from the glacial diamictites from this study; the corresponding MgO contents are from Tang et al. (2016). The uncertainty of Paleozoic UCC Cu/Ag (200 ± 200) is not shown in the figure because it plots off the scale.

komatiites and basalts, the high and moderate degree partial melts of the mantle, respectively, should also have similar Cu/Ag ratios to mantle and MORB values (~3500). Given that sulfide is undersaturated during the fractionation of komatiitic and basaltic magmas (Fig. 1), Cu and Ag should partition into the melts, producing limited variation of Cu/Ag ratios in komatiites and basalts with lower MgO contents. Therefore, both komatiites and basalts are assumed to have similar Cu/Ag ratios to the mantle value, as represented by fertile peridotites ($Al_2O_3 > 2\%$), which have an average Cu/Ag ratio of 3400 ± 300 (n = 36, 2SE) (Wang and Becker, 2015).

By contrast, felsic rocks in back-arc basins generally have much lower Cu/Ag ratios of 200–500 (Fig. 7) (Jenner et al., 2010, 2012), which is caused by crystalline sulfide fractionation during the late stage differentiation of back-arc basin magmas (Jenner, 2017) because Cu is more compatible than Ag in crystalline sulfides (Li and Audétat, 2012; Zajacz et al., 2013). This crystalline sulfide fractionation has been suggested to be caused by the so called "magnetite crisis" (Jenner et al., 2010; Jenner, 2017). The low Cu/Ag ratios have also been observed in felsic rocks from East China (with a median of ~240 ± 70, n = 27, Fig. 7, Table A1, Gao et al., 1998) and felsic glasses from Hawaii lavas (100–700, Fig. 7, Greaney et al., 2017). Knowing the Cu/Ag ratios and relative proportions of the three major rock types for the UCC over time, we can calculate the weighted average Cu/Ag ratio for the corresponding UCC and compare the results with the Cu/Ag ratios in the diamictite samples.

Thus, for the ~2.5 Ga or ~3.0 Ga UCC, we have the following equations:

$$\frac{C_k^{Cu}}{C_k^{Ag}} = \frac{C_b^{Cu}}{C_b^{Ag}} = 3400 \pm 300 \qquad \frac{C_f^{Cu}}{C_f^{Ag}} = 240 \pm 70 \tag{3}$$

$$\frac{F_k C_k^{Cu} + F_b C_b^{Cu} + F_f C_f^{Cu}}{F_k C_k^{Ag} + F_b C_b^{Ag} + F_f C_f^{Ag}} = \frac{C_{UCC}^{Cu}}{C_{UCC}^{Ag}} \tag{4}$$

$$F_k + F_b + F_f = 1 \tag{5}$$

where C_{UCC}^{Cu} and C_{UCC}^{Ag} are the average Cu and Ag concentrations for the UCC, respectively. Using the F_k, F_b and F_f obtained in Section 5.2.1, we calculate that the weighted average Cu/Ag ratio is between 2200 and 3400 for the ~3.0 Ga UCC and 900 ± 200 for the ~2.4 Ga and younger UCC. Considering uncertainties, these Cu/Ag ratios are in agreement with the median Cu/Ag ratios of the Mesoarchean and the younger diamictites, which are 2100 ± 600 and 200–700, respectively (Table 4). Thus, our Cu/Ag ratio calculations support the lithological proportion results obtained from the Cu mass-balance calculations.

5.2.3. Major elements in the UCC

Based on the lithological proportions obtained using Cu mass balance and the average MgO and SiO_2 contents of various lithologies (Table 3), we reconstruct average MgO and SiO_2 contents of the UCC through time (Fig. 8). The results show that the MgO content decreased from 6-14 wt.% around 3.0 Ga ago to 2–3 wt.% around 2.4 Ga ago, coupled with an increase of SiO_2 content from 48-

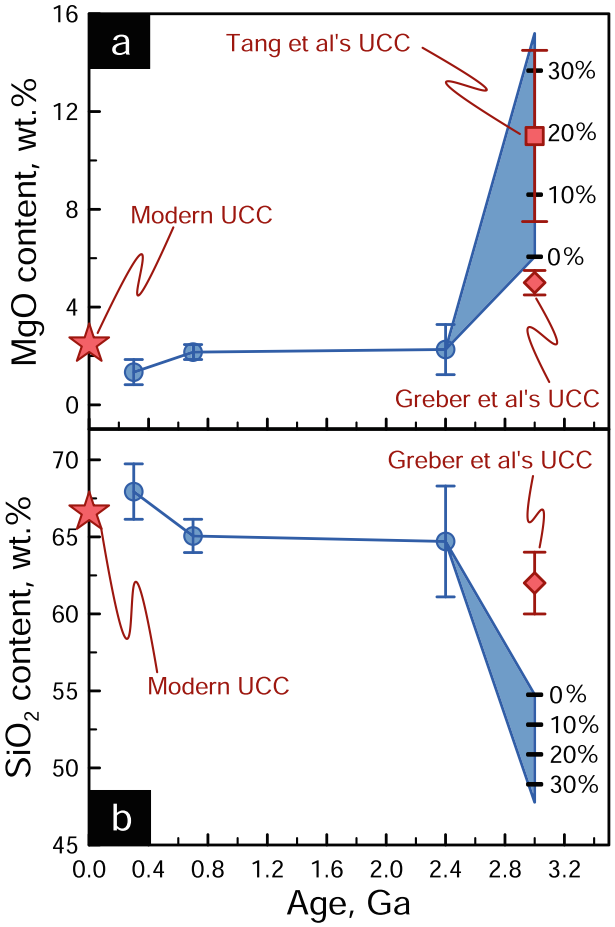

Fig. 8. Constructed average MgO and SiO_2 contents in the UCC through time. Lithological proportions are from Cu mass balance and the average MgO and SiO_2 contents for komatiites, basalts and felsic rocks are from Table 3. The black numbers, 0%, 10%, 20% and 30% are the proportions of komatiite in the Mesoarchean UCC. Shown for comparison are the estimates of average Archean UCC from Tang et al. (2016) and Greber et al. (2017).

54 wt.% to 64–65 wt.%, consistent with a mafic-to-felsic transition of the UCC during the late Archean. Based on the estimated lithological proportions and the average contents of the major elements in the three lithologies (Table A3), we also calculated the average contents of other major elements in the UCC (Table A4).

Our estimate of the Archean UCC composition is consistent with that proposed by Tang et al. (2016) and supports the hypothesis that the UCC transitioned from a mafic-rock-dominated to a felsic-rock-dominated bulk composition between ~3.0 and ~2.4 Ga (Tang et al., 2016; Smit and Mezger, 2017). The findings stand in contrast to the results inferred from shale Ti isotope (Greber et al., 2017) and Al_2O_3/TiO_2 and Zr/TiO_2 ratios in terrigenous sediments (Greber and Dauphas, 2019). We suggest that the discrepancy may be largely due to the uncertainty in the pathways of Archean igneous differentiation (e.g., calc-alkaline vs. tholeiitic); Ti, in particular (both concentrations and isotopes), behaves very differently between these two differentiation suites, producing distinct $\delta^{49}Ti$–SiO_2, Zr/TiO_2–SiO_2 and Al_2O_3/TiO_2–SiO_2 correlations in rocks produced in different tectonic settings (e.g., Deng et al., 2019; Fig. A4). For example, in contrast to the conclusions of Greber and Dauphaus (2019), we find that the Zr/TiO_2–SiO_2 and Al_2O_3/TiO_2-SiO_2 relationships differ between calc-alkaline Andean arc and tholeiitic Icelandic magmas (Fig. A4), which means that these ratios, like $\delta^{49}Ti$, are not unique proxies for average SiO_2 content of the UCC. Because we do not know the tectonic settings for most Archean igneous suites, elemental and isotope ratios showing non-unique relationships with SiO_2 during igneous differentiation (e.g., Al_2O_3/TiO_2, Zr/TiO_2, and $\delta^{49}Ti$) cannot be used to infer the average SiO_2 content of the Archean UCC. Further complexities in applying Ti isotopes to shales may come from Ti isotope fractionation during chemical weathering (Aarons et al., 2018).

5.3. Insights into Archean dynamic regimes and surface environment

The fundamental change in UCC composition that occurred during the late Archean requires prodigious production of granitic rocks (Tang et al., 2016). Although the processes for generating granitic magmas in the Archean remain contentious (slab melting vs. thickened crustal melting, Albarède, 1998; Smithies, 2000; Foley et al., 2002; Martin and Moyen, 2002; Rapp et al., 2003; Bédard, 2006), water is critical in granite formation (Campbell and Taylor, 1983; Arndt, 2013; Lee et al., 2015), and subduction appears to be the most efficient way of transporting water from Earth's surface to its interior. We thus suggest that late Archean crustal evolution was primarily driven by widespread subduction, likely marking the onset of plate tectonics (Dhuime et al., 2015; Lee et al., 2016; Tang et al., 2016).

The transition from Fe- and Mg-rich mafic rocks to feldspar- and quartz-rich felsic rocks in the exposed crust during the late Archean may exert a large influence on the chemical composition of the atmosphere. Atmospheric oxygen levels rose significantly around 2.4–2.2 Ga ago, which is known as the Great Oxidation Event (GOE, Holland, 2002). The atmosphere oxygen level is governed by the balance between O_2 production (oxygenic photosynthesis) and consumption (reaction with reductants, e.g., hydrogen, methane, organic carbon, sulfides and ferrous iron). By replacing an Fe^{2+} and S^{2-} rich mafic crust with an Fe^{2+} and S^{2-} poor felsic crust, the reducing power of the crust could be greatly diminished (Lee et al., 2016). Related effects include reduction in the continental Ni flux to the oceans, which, because Ni is an essential micronutrient for methanogens, would have reduced methane production, thus decreasing a key oxygen sink (Konhauser et al., 2009). In addition, the expansion of subaerial crust associated with massive continent growth may have also enhanced the flux of organic carbon burial on continental shelves and CO_2-silicate reactions, leading to net O_2 production (Husson and Peters, 2017) and stronger chemical weathering feedbacks (Lee et al., 2017). The rapid emergence of subaerial crust may have also driven the onset of the modern hydrologic cycle, as recorded by a shift in triple

oxygen isotope compositions in shales at the end of Archean (Bindeman et al., 2018), and fundamentally changed the chemical fluxes from the continents to the oceans.

6. CONCLUSIONS

Magma [Cu] is strongly controlled by sulfide saturation during partial melting and differentiation. As a consequence, basaltic rocks generally have higher [Cu] than ultramafic and felsic rocks, making the Cu budget in the UCC highly sensitive to the amount of basalts. The unique Cu–MgO relationship allows us to track the proportion of mafic compositions and thus the bulk composition of UCC through time.

We quantified the evolution the UCC [Cu] through time by measuring glacial diamictites with depositional ages from ~3.0 to ~0.3 Ga. Because Cu is a relatively insoluble element, its concentration will not be significantly influenced by chemical weathering. We found that the UCC had a high [Cu] of ~64 ppm in the Mesoarchean and then its [Cu] plummeted to ~24 ppm and has remained constant since the Paleoproterozoic. The Mesoarchean UCC had a higher [Cu] than both Archean komatiites and felsic rocks and was only lower than Archean basalts, which requires basalts to be the dominant lithology (65–75%) in the UCC at that time. The low [Cu] in the Paleoproterozoic diamictites suggest that the UCC became dominated by felsic rocks (~70%) at the end of the Archean. This rapid change in UCC composition in the late Archean is also supported by the secular change in Cu/Ag ratio of diamictites. Our findings of UCC [Cu] evolution suggest that fundamental changes of the UCC composition occurred at 3.0–2.4 Ga, which may be linked to the start of Wilson cycle in the late Archean.

ACKNOWLEDGEMENTS

This work was supported by the National Natural Science Foundation of China (41703034), the 111 Project from Chinese Ministry of Education (BP0719022), the State Key Laboratory of Geological Processes and Mineral Resources (MSFGPMR12, MSFGPMR02-1), and NSF (EAR 1321954). We thank Yinuo Liu for her help on column chemistry. We thank Frances Jenner and two anonymous reviewers for their constructive comments that helped us to improve the paper.

APPENDIX A. SUPPLEMENTARY MATERIAL

Appendix materials (Figs. A1, A2, A3 and A4, and Tables A1, A2, A3 and A4) associated with this article can be found in the online version. Supplementary data to this article can be found online at https://doi.org/10.1016/j.gca.2019.08.002.

REFERENCES

Aarons S. M., Dauphas N., Teng F.-Z., Liu X., Rudnick R. L., Bouchez J. and Gaillardet J. (2018) Preliminary investigation of Ti transport and isotopic fractionation in the critical zone. In *AGU Fall Meeting, Washington, D.C.*, pp. H23P–H2183.

Adam J. and Green T. (2006) Trace element partitioning between mica- and amphibole-bearing garnet lherzolite and hydrous basanitic melt: 1. Experimental results and the investigation of controls on partitioning behaviour. *Contrib. Mineral. Petrol.* **152**, 1–17.

Albarède F. (1998) The growth of continental crust. *Tectonophysics* **296**, 1–14.

Arndt N. (2003) Komatiites, kimberlites, and boninites. *J. Geophys. Res.: Solid Earth* **108**.

Arndt N., Lesher M. C. and Barnes S. J. (2008). *Komatiite*.

Arndt N. T. (2013) Formation and evolution of the continental crust. *Geochem. Perspect.* **2**, 405–533.

Bédard J. H. (2006) A catalytic delamination-driven model for coupled genesis of Archaean crust and sub-continental lithospheric mantle. *Geochim. Cosmochim. Acta* **70**, 1188–1214.

Bindeman I. N., Zakharov D. O., Palandri J., Greber N. D., Dauphas N., Retallack G. J., Hofmann A., Lackey J. S. and Bekker A. (2018) Rapid emergence of subaerial landmasses and onset of a modern hydrologic cycle 2.5 billion years ago. *Nature* **557**, 545–548.

Boyle E. A., Sclater F. R. and Edmond J. M. (1977) The distribution of dissolved copper in the Pacific. *Earth Planet. Sci. Lett.* **37**, 38–54.

Broecker W. S. and Peng T.-H. (1982) Tracers in the Sea. Lamont-Doherty Geological Observatory, 690.

Campbell I. H. and Taylor S. R. (1983) No water, no granites - No oceans, no continents. *Geophys. Res. Lett.* **10**, 1061–1064.

Chen K., Walker R. J., Rudnick R. L., Gao S., Gaschnig R. M., Puchtel I. S., Tang M. and Hu Z.-C. (2016) Platinum-group element abundances and Re–Os isotopic systematics of the upper continental crust through time: Evidence from glacial diamictites. *Geochim. Cosmochim. Acta* **191**, 1–16.

Condie K. C. (1993) Chemical composition and evolution of the upper continental crust: Contrasting results from surface samples and shales. *Chem. Geol.* **104**, 1–37.

Condie K. C. (1994) Chapter 3 greenstones through time. In *Developments in Precambrian Geology* (ed. K. C. Condie). Elsevier, pp. 85–120.

Deng Z., Chaussidon M., Savage P., Robert F., Pik R. and Moynier F. (2019) Titanium isotopes as a tracer for the plume or island arc affinity of felsic rocks. *Proc. Natl. Acad. Sci.* **116**, 1132.

Dhuime B., Wuestefeld A. and Hawkesworth C. J. (2015) Emergence of modern continental crust about 3 billion years ago. *Nat. Geosci.* **8**, 552–555.

Ewart A. and Griffin W. L. (1994) Application of proton-microprobe data to trace-element partitioning in volcanic rocks. *Chem. Geol.* **117**, 251–284.

Foley S., Tiepolo M. and Vannucci R. (2002) Growth of early continental crust controlled by melting of amphibolite in subduction zones. *Nature* **417**, 837–840.

Gao S., Luo T. C., Zhang B. R., Zhang H. F., Han Y. W., Zhao Z. D. and Hu Y. K. (1998) Chemical composition of the continental crust as revealed by studies in East China. *Geochim. Cosmochim. Acta* **62**, 1959–1975.

Gaschnig R. M., Rudnick R. L., McDonough W. F., Kaufman A. J., Hu Z. and Gao S. (2014) Onset of oxidative weathering of continents recorded in the geochemistry of ancient glacial diamictites. *Earth Planet. Sci. Lett.* **408**, 87–99.

Gaschnig R. M., Rudnick R. L., McDonough W. F., Kaufman A. J., Valley J. W., Hu Z., Gao S. and Beck M. L. (2016) Compositional evolution of the upper continental crust through time, as constrained by ancient glacial diamictites. *Geochim. Cosmochim. Acta* **186**, 316–343.

Greaney A. T., Rudnick R. L., Helz R. T., Gaschnig R. M., Piccoli P. M. and Ash R. D. (2017) The behavior of chalcophile

elements during magmatic differentiation as observed in Kilauea Iki lava lake, Hawaii. *Geochim. Cosmochim. Acta* **210**, 71–96.
Greber N. D., Dauphas N., Bekker A., Ptáček M. P., Bindeman I. N. and Hofmann A. (2017) Titanium isotopic evidence for felsic crust and plate tectonics 3.5 billion years ago. *Science* **357**, 1271–1274.
Greber N. D. and Dauphas N. (2019) The chemistry of fine-grained terrigenous sediments reveals a chemically evolved Paleoarchean emerged crust. *Geochim. Cosmochim. Acta* **255**, 247–264.
Hamaguchi H. and Kuroda R. (1959) Silver content of igneous rocks. *Geochim. Cosmochim. Acta* **17**, 44–52.
Holland H. D. (2002) Volcanic gases, black smokers, and the great oxidation event. *Geochim. Cosmochim. Acta* **66**, 3811–3826.
Horton T. W., Chamberlain C. P., Fantle M. and Blum J. D. (1999) Chemical weathering and lithologic controls of water chemistry in a high-elevation river system: Clark's Fork of the Yellowstone River, Wyoming and Montana. *Water Resour. Res.* **35**, 1643–1655.
Hu Z. and Gao S. (2008) Upper crustal abundances of trace elements: A revision and update. *Chem. Geol.* **253**, 205–221.
Husson J. M. and Peters S. E. (2017) Atmospheric oxygenation driven by unsteady growth of the continental sedimentary reservoir. *Earth Planet. Sci. Lett.* **460**, 68–75.
Jenner F. E., O'Neill H. S. C., Arculus R. J. and Mavrogenes J. A. (2010) The magnetite crisis in the evolution of arc-related magmas and the initial concentration of Au, Ag and Cu. *J. Petrol.* **51**, 2445–2464.
Jenner F. E., Arculus R. J., Mavrogenes J. A., Dyriw N. J., Nebel O. and Hauri E. H. (2012) Chalcophile element systematics in volcanic glasses from the northwestern Lau Basin. *Geochem. Geophys. Geosyst.* **13**, Q06014.
Jenner F. E. and O'Neill H. S. C. (2012) Analysis of 60 elements in 616 ocean floor basaltic glasses. *Geochem. Geophys. Geosyst.* **13**, Q02005.
Jenner F. E. (2017) Cumulate causes for the low contents of sulfide-loving elements in the continental crust. *Nat. Geosci.* **10**, 524–529.
Johnson B. W. and Goldblatt C. (2017) A secular increase in continental crust nitrogen during the Precambrian. *Geochem. Perspect. Lett.* **4**, 24–28.
Keller C. B., Schoene B., Barboni M., Samperton K. M. and Husson J. M. (2015) Volcanic-plutonic parity and the differentiation of the continental crust. *Nature* **523**, 301–307.
Konhauser K. O., Pecoits E., Lalonde S. V., Papineau D., Nisbet E. G., Barley M. E., Arndt N. T., Zahnle K. and Kamber B. S. (2009) Oceanic nickel depletion and a methanogen famine before the Great Oxidation Event. *Nature* **458**, 750–753.
Lee C.-T. A., Luffi P., Chin E. J., Bouchet R., Dasgupta R., Morton D. M., Le Roux V., Yin Q.-Z. and Jin D. (2012) Copper systematics in arc magmas and implications for crust-mantle differentiation. *Science* **336**, 64–68.
Lee C.-T. A., Morton D. M., Farner M. J. and Moitra P. (2015) Field and model constraints on silicic melt segregation by compaction/hindered settling: The role of water and its effect on latent heat release. *Am. Mineral.* **100**, 1762–1777.
Lee C.-T. A., Yeung L. Y., McKenzie N. R., Yokoyama Y., Ozaki K. and Lenardic A. (2016) Two-step rise of atmospheric oxygen linked to the growth of continents. *Nat. Geosci.* **9**, 417–424.
Lee C.-T. A., Caves J., Jiang H., Cao W., Lenardic A., McKenzie N. R., Shorttle O., Yin Q.-Z. and Dyer B. (2017) Deep mantle roots and continental emergence: implications for whole-Earth elemental cycling, long-term climate, and the Cambrian explosion. *Int. Geol. Rev.*, 1–18.
Li S., Gaschnig R. M. and Rudnick R. L. (2016) Insights into chemical weathering of the upper continental crust from the geochemistry of ancient glacial diamictites. *Geochim. Cosmochim. Acta* **176**, 96–117.
Li Y. and Audétat A. (2012) Partitioning of V, Mn Co, Ni, Cu, Zn, As, Mo, Ag, Sn, Sb, W, Au, Pb, and Bi between sulfide phases and hydrous basanite melt at upper mantle conditions. *Earth Planet. Sci. Lett.* **355–356**, 327–340.
Martin H. and Moyen J. F. (2002) Secular changes in tonalite-trondhjemite-granodiorite composition as markers of the progressive cooling of Earth. *Geology* **30**, 319–322.
McLennan S. M. (1993) Weathering and global denudation. *J. Geol.* **101**, 295–303.
Middelburg J. J., van der Weijden C. H. and Woittiez J. R. W. (1988) Chemical processes affecting the mobility of major, minor and trace elements during weathering of granitic rocks. *Chem. Geol.* **68**, 253–273.
Mundl A., Walker R. J., Reimink J. R., Rudnick R. L. and Gaschnig R. M. (2018) Tungsten-182 in the upper continental crust: Evidence from glacial diamictites. *Chem. Geol.* **494**, 144–152.
Nan X.-Y., Yu H.-M., Rudnick R. L., Gaschnig R. M., Xu J., Li W.-Y., Zhang Q., Jin Z.-D., Li X.-H. and Huang F. (2018) Barium isotopic composition of the upper continental crust. *Geochim. Cosmochim. Acta* **233**, 33–49.
Nesbitt H. W. and Young G. M. (1982) Early Proterozoic climates and plate motion inferred from major element chemistry of lutites. *Nature* **299**, 715–717.
Nesbitt H. W. and Wilson R. E. (1992) Recent chemical weathering of basalts. *Am. J. Sci.* **292**, 740–777.
Nesbitt W. H. and Markovics G. (1997) Weathering of granodioritic crust, long-term storage of elements in weathering profiles, and petrogenesis of siliciclastic sediments. *Geochim. Cosmochim. Acta* **61**, 1653–1670.
O'Neil J. and Carlson R. W. (2017) Building Archean cratons from Hadean mafic crust. *Science* **355**, 1199–1202.
Rapp R. P., Shimizu N. and Norman M. D. (2003) Growth of early continental crust by partial melting of eclogite. *Nature* **425**, 605–609.
Reekie C. D. J., Jenner F. E., Smythe D. J., Hauri E. H., Bullock E. S. and Williams H. M. (2019) Sulfide resorption during crustal ascent and degassing of oceanic plateau basalts. *Nat. Commun.* **10**, 82.
Reimink J. R., Chacko T., Carlson R. W., Shirey S. B., Liu J., Stern R. A., Bauer A. M., Pearson D. G. and Heaman L. M. (2018) Petrogenesis and tectonics of the Acasta Gneiss Complex derived from integrated petrology and 142Nd and 182W extinct nuclide-geochemistry. *Earth Planet. Sci. Lett.* **494**, 12–22.
Rudnick R. L. (1995) Making continental crust. *Nature* **378**, 571–578.
Rudnick R. L. and Gao S. (2003) 3.01 - Composition of the continental crust. In *Treatise on Geochemistry* (eds. H. D. Holland and K. K. Turekian), first ed. Pergamon, Oxford, pp. 1–64.
Smit M. A. and Mezger K. (2017) Earth's early O2 cycle suppressed by primitive continents. *Nat. Geosci.* **10**, 788.
Smithies R. H. (2000) The Archaean tonalite-trondhjemite-granodiorite (TTG) series is not an analogue of Cenozoic adakite. *Earth Planet. Sci. Lett.* **182**, 115–125.
Tang M., Chen K. and Rudnick R. L. (2016) Archean upper crust transition from mafic to felsic marks the onset of plate tectonics. *Science* **351**, 372–375.
Taylor S. R. and McLennan S. M. (1985) *The Continental Crust: its Composition and Evolution*. Blackwell Scientific, Oxford.

Wang S.-J., Rudnick R. L., Gaschnig R. M., Wang H. and Wasylenki L. E. (2019) Methanogenesis sustained by sulfide weathering during the great oxidation event. *Nat. Geosci.* **12**, 296–300.

Wang Z. and Becker H. (2013) Ratios of S, Se and Te in the silicate Earth require a volatile-rich late veneer. *Nature* **499**, 328–331.

Wang Z. and Becker H. (2015) Abundances of Ag and Cu in mantle peridotites and the implications for the behavior of chalcophile elements in the mantle. *Geochim. Cosmochim. Acta* **160**, 209–226.

Wang Z., Becker H. and Wombacher F. (2015) Mass fractions of S, Cu, Se, Mo, Ag, Cd, In, Te, Ba, Sm, W, Tl and Bi in geological reference materials and selected carbonaceous chondrites determined by isotope dilution ICP-MS. *Geostand. Geoanal. Res.* **39**, 185–208.

Wang Z., Becker H., Liu Y., Hoffmann E., Chen C., Zou Z. and Li Y. (2018a) Constant Cu/Ag in upper mantle and oceanic crust: Implications for the role of cumulates during the formation of continental crust. *Earth Planet. Sci. Lett.* **493**, 25–35.

Wang Z., Ma J., Li J., Wei G., Zeng T., Li L., Zhang L., Deng W., Xie L. and Liu Z. (2018b) Fe (hydro) oxide controls Mo isotope fractionation during the weathering of granite. *Geochim. Cosmochim. Acta* **226**, 1–17.

Wedepohl K. H. (1995) The composition of the continental crust. *Geochim. Cosmochim. Acta* **59**, 1217–1232.

Wilson M. (1989) *Igneous Petrogenesis: A Global Tectonic Approach*. Springer, p. 466.

Yang S., Humayun M. and Salters V. J. M. (2018) Elemental systematics in MORB glasses from the Mid-Atlantic Ridge. *Geochem., Geophys., Geosyst.*, 2018GC007593.

Zajacz Z., Candela P. A., Piccoli P. M., Sanchez-Valle C. and Wälle M. (2013) Solubility and partitioning behavior of Au, Cu, Ag and reduced S in magmas. *Geochim. Cosmochim. Acta* **112**, 288–304.

Zakharova E. A., Pokrovsky O. S., Dupré B., Gaillardet J. and Efimova L. E. (2007) Chemical weathering of silicate rocks in Karelia region and Kola peninsula, NW Russia: Assessing the effect of rock composition, wetlands and vegetation. *Chem. Geol.* **242**, 255–277.

Associate editor: Fang-Zhen Teng